Day-to-day variability and solar preconditioning of thermospheric temperature over Millstone Hill

Day-to-day Variability and Solar Preconditioning of Thermospheric Temperature over Millstone Hill

Shun-Rong Zhang, John M. Holt, Philip J. Erickson, Larisa P. Goncharenko

MIT Haystack Observatory, Westford, Massachusetts, USA

S.-R. Zhang, J. M. Holt, P. J. Erickson, and L. P. Goncharenko, Haystack Observatory, Massachusetts Institute of Technology, Route 40, Westford, MA 01886. (shunrong@haystack.mit.edu)

Abstract.

We use a continuous 30 day incoherent scatter radar experiment at Millstone Hill in October 2002 to examine day-to-day thermospheric variability in exospheric temperature T_{ex}. Solar flux and magnetic activity influences as the main driving factors for day-to-day variability are investigated quantitatively. Solar ultraviolet flux levels are based on the TIMED/SEE space weather product, allowing for analysis of ultraviolet flux-T_{ex} correlation. T_{ex} is most sensitive to solar EUV flux with approximately a 2-day delay at wavelengths of 27–34 nm (including 30.4 nm). In particularly, a 20–60-hour time delay occurs in T_{ex} response to EUV flux at 27-34 nm band, with shorter delays in the morning and longer delays in the afternoon and at night. The 1∼2-day delayed T_{ex} response to solar ultraviolet flux and associated thermospheric solar preconditioning ("memory") are most significant in the daily mean for the 27-34 nm band, in the diurnal and semidiurnal amplitudes for the soft X-ray flux at 0.1–7 nm, and in the diurnal amplitude for longer wavelengths. An empirical model driven only by EUV flux at 27–34 nm from two days in advance reproduces 90% of the observed variability in the T_{ex} daily mean. With a two-day time delay, solar X-ray flux at 0.1–7 nm is correlated positively with T_{ex} diurnal amplitude, and negatively with T_{ex} semidiurnal amplitude. Finally, magnetic activity control, as represented by the Dst index, is weaker during the day and stronger at night, and is important for the semidiurnal amplitude but not important for the daily mean.

1. Introduction

Variability in the physical state of the upper atmosphere can be significant but in general is not well understood. Some progress has recently been achieved primarily in characterizing variability in ionospheric electron density (see Rishbeth and Mendillo [2001]) and plasma temperatures (see Zhang and Holt [2008]). However, variability in thermospheric parameters, and in particular their day-to-day variability, has been less pursued due to the relatively fewer observations available. Advancing knowledge of thermospheric variability is very important not only for understanding of the neutral atmosphere but also of the ionosphere, since the relatively smaller plasma densities in the ionosphere are embedded in and heavily influenced by the much larger neutral densities in the thermosphere. Thus, thermosphere variability provides a major source of ionospheric variability. The ionospheric plasma is created through photoionization of neutrals, with losses to the neutral atmosphere and whose kinematics are directly under the influence of ion-neutral collision. Solar irradiation and magnetic activity are the main direct external drivers of thermospheric variability. Various thermospheric momentum and energetic processes such as acoustic, tidal, and planetary waves, as well as meteorological processes can result in thermospheric variability due to coupling between different atmospheric layers, imposing significant impacts on the ionosphere (Forbes and Zhang [1997], Forbes [2000], Rishbeth and Mendillo [2001], Altadill and Apostolov [2001], Mendillo et al. [2002], Laštovička [2006], Rishbeth [2006], Goncharenko et al. [2010]).

An incoherent scatter radar (ISR) is one of the very few instruments that can be used to monitor thermospheric variations from the ground, through observations of ionospheric

parameters combined with energy balance equations. A well-established method for deriving the neutral temperature profile originated in work by Bauer et al. [1970] based on energy balance equations for ionic species, and is still being used (e.g. Nicolls et al. [2006]). Many prior ISR observations of exospheric temperature were used as a major source of data for climatology and detailed temporal variations used to construct the MSIS neutral atmospheric models (Hedin [1987]; Picone et al. [2002]). Millstone Hill ISR observations were first used by Salah and Evans [1973] to conduct thermospheric temperature studies. Most prior studies on exospheric temperature involve climatology derived from a variety of solar-geophysical conditions. For example, Hagan and Oliver [1985] uses ISR data to examine thermospheric solar cycle variability. Oliver and Salah [1988] reported results of the Global Thermospheric Mapping Study (GTMS) campaigns, which covered two 3-day periods. Buonsanto and Pohlman [1998] examined exospheric temperature climatology above Millstone Hill, and Oliver [1997] uses similar observations to focus on the O^+-O collision cross-section. Other techniques have also been developed to extract information of the thermospheric temperature from ISR measurements, e.g. data assimilation approaches using electron density profiles [Zhang et al, 2001; Mikhailov and Lilensten, 2004] along with key ionospheric parameters [Zhang et al, 2003]. These data assimilation approach techniques are applicable for electron density observations obtained by techniques other than ISR (e.g. ionosonde). However, in this paper we focus on the energy balance method using as input ISR measurements of plasma temperatures T_i and T_e, in addition to electron density N_e.

While ground-based observations are relatively few for thermospheric studies, long time series of ground-based thermospheric temperature observations sufficient for day-to-day

variability investigations are truly rare but do exist. Using an unique dataset from October 2002 providing a consecutive 30-day ISR exospheric temperature observation at Millstone Hill, the present paper deals with day-to-day variability of the thermosphere at medium to high solar activity. Ionospheric variability during this long duration ISR experiment was discussed previously. Zhang et al. [2005] found quasi-periodic electron density oscillations with periods >1 day. While some of those fluctuations were correlated with changes in the neutral composition originating from geomagnetic activity, the wave-like oscillations in electron density exhibited phase changes with height which persists up to 600 km and prevailed until a large storm appears to impose a phase change in an opposite direction. In a study of the E-region variability, Moore et al. [2006] noted that photochemical modeling can reproduce the electron density variability at mid- and low-latitudes, and the variability is dominated mostly by solar flux variations, modified by solar declination, and least affected by neutral density changes. In an analysis of another 30-day ISR experiment at Millstone Hill (September 2005), Zhang and Holt [2008] indicated that with increasing solar flux, electron density decreases between 170 km and the F2 peak and increases elsewhere, being essentially unchanged near the F2 peak. A time lag of ionospheric responses to changes in the 10.7 cm solar flux was also found: in the E region, the lag is almost zero; above the F2 peak, the lag for either electron density or ion temperature is $\sim$2 days.

Here, we characterize thermospheric day-to-day variability during geomagnetic quiet conditions, where solar flux is a dominant day-to-day variability driver. In addition to the traditional 10.7 cm solar flux proxy, we focus on different effects of EUV/FUV flux at various wavelength bands, including the time delay of thermospheric responses to solar flux

and issues related to thermospheric solar preconditioning or so-called "memory" [Rishbeth, 2007]. We also study thermospheric temperature changes in response to frequent weak to moderate magnetic activity, and quantitatively gauge relative contributions of solar flux and magnetic activity conditions to the observed temperature variability.

2. Solar geophysical conditions and ISR measurements of plasma parameters

From October 4 to November 4, 2002, a consecutive 30-day incoherent scatter radar (ISR) campaign was conducted at Millstone Hill (42.6°N, 288.5°E, Invariant Lat. 53.4°), using a high power large aperture UHF radar system at MIT Haystack Observatory. The radar's 68-m diameter zenith antenna was used to measure at 4 minute cadence vertical profiles of electron density Ne, electron temperature T_e , ion temperature T_i , and line-of-sight velocity Vo. A set of interleaved single pulses and alternating-coded pulses provided E and F region ionospheric observations with an altitude resolution ranging from 4.5 km (E region) to >40 km (F region).

During this period, the 10.7 cm solar flux proxy F107 varied between 155 to 185 units (1 unit = 10^{22} W m^{-2} Hz^{-1}) from October 4 to November 4, 2002 (day number = 277 to 308) whereas its 81-day average was around 169 units, peaked at 174 units on day 283, and decreased in general toward the end of the period reaching a minimum of 164 units on day 306. The F107 proxy, which was larger near the middle of the month, also showed a gradual change with a 27-day periodicity due to solar synodical rotation. Magnetic disturbances were noticeable only on three occasions. On October 7 (day 280), the hourly Dst index [Sugiura , 1964] dropped to -100 nT where it stayed for about 1 full day before it recovered. On October 14 (day 287), a sharp and brief drop in Dst to a minimum of -100 nT occurred. On October 24 (day 297), a major storm was launched with a Dst

minimum of -90 nT, main phase of 12 hours and recovery phase of several days, causing severe ionospheric storms. Detailed information about the daily solar 10.7 cm radio flux index F107, hourly Dst index, and 3-hourly ap index are shown in Figure 1 of Zhang et al. [2005]. In this current paper, our primary interest is day-to-day variability not apparently associated with strong magnetic activity (already investigated extensively by numerous researchers). Therefore, we select data with hourly Dst >-75 nT at any given time, and furthermore where, immediately prior to the current time, 6-hourly and 3-hourly average Dst values > -60 nT. These -60/-75 nT bounds were determined based on examining the histogram of Dst data for the entire period, so that enough data points are available for robust statistics while observations with medium to high magnetic activity are effectively eliminated. These bounds are slightly smaller but close to the typical -50 nT threshold for classification of moderate to intense storms (cf. Wanliss and Showalter [2006] for results from a very large dataset from 1963 to 2002).

The method for deriving $T_n(z)$ (and neutral oxygen density) is based on the ion energy balance equation. Bauer et al. [1970], Salah and Evans [1973], Alcaydé et al. [1982], and most recently Nicolls et al. [2006] describe methods in some detail which are valid for the F2 region. The Oliver [1979] method is an extension of these techniques down to the lower F region and the E-region, and determines additional quantities as well as providing modest improvements in the profile shape of the neutral temperature. The present paper will adopt this latter method since our alternating code measurements at 4.5 km minimum altitude resolution provide excellent E and lower-F region data during this campaign. The Oliver [1979] method assumes that the ions are heated by Coulomb collisions with electrons and cooled by elastic collisions with neutrals. The energy transfer coefficients are

proportional to number densities of the involved particles, including in particular, oxygen ion density [O^+] and oxygen density [O]. However, T_n(z) is calculated from this energy equation through a profile fit to a Bates function-type height variation. In this function, T_n(z) is determined by three parameters: the thermo-base temperature T_b for 120 km, the exospheric temperature T_{ex} and the shape factor s determining how fast T_n approaches T_{ex} from T_b, i.e., $T_n(z)=T_{ex}-(T_{ex}-T_b)\exp[-sz_g(z)]$, with z_g(z) being geopotential height. In fact, $1/s$, the inverse of the shape factor, is equivalent to scale height with units of km. Atomic oxygen is assumed to be in diffusive equilibrium, so [O] is determined by neutral temperature and the oxygen density at a reference height, normally set at 400 km. Neutral quantities needed for the energy equation calculations are obtained using the NRL-MSIS model [Picone et al., 2002]. The 4 parameters [T_{ex}, T_b, s and $[O]_{400km}$] are inserted into the energy equation (through T_n and [O]) and then T_i is calculated. The best set of the 4 parameters is chosen in a least squares sense, such that the calculated T_i profile best fits the measured T_i profile. In practice, we set [O] to MSIS values, as our fit results along with previous work on this algorithm [Litvin et al., 2000] indicate that the resulting T_{ex} is hardly affected by values of [O]. Similarly, O^+-O collision cross-section is not an important parameter for the T_{ex} study reported here, although it can be important for determining the absolute value of [O] as the temperature-density product defines energy transfer coefficients from O^+ to atomic oxygen [Oliver and Glotfelty, 1996].

Determination of T_b and s is sensitive in particular to measurements in the E region. In practice, midlatitude E region electron density is low at night leading to weak detected ISR signals and high measurement uncertainty in the resulting plasma parameters. Therefore, nighttime T_b and s data may be considered as first order quantities while corresponding

T_{ex} is zeroth order quantity. Additionally, nighttime conditions have a lack of significant photoionization, and therefore strong heat coupling among plasma and neutrals leads to approximately equal T_i, T_e and T_n values, increasing the difficulty of determining neutral temperature from the detected plasma temperature.

There are two main assumptions involved in the somewhat simplified energy equation method used in this study. First, frictional heating is ignored. In cases where frictional heating is large enough, Litvin et al. [2000] shows that neutral temperature may be underestimated. Since we have selected data for relatively quiet magnetic activity as mentioned earlier, we do not expect our results to be significantly affected by frictional heating. Second, thermal conduction is ignored, and it is known that thermal conduction may become significant in the upper F region. However, this assumption would not affect our T_{ex} results significantly, because they are essentially determined by data below 300 km where the ions and neutrals are in close thermal contact and thermal conduction is not important. Therefore the accuracy of T_n depends strongly on the quality of the observed T_i, with a typical measurement uncertainty of 10-30 K (varying with geophysical conditions and observational facility systems). At this uncertainty level, Nicolls et al. [2006], using a least squares fit matching the energy transfer rate between electrons to the ions with the rate between the ions to the neutrals, provided a detailed error analysis for Arecibo incoherent scatter radar observations. The resulting fractional error in T_{ex} was found typically within 0.01, equivalent to 10-20 K for the geophysical conditions in this study.

3. Day-to-day thermospheric variability

Diurnal variations and their variability for the set of three derived thermospheric parameters [T_{ex}, T_b, $1/s$] over the 30-day October 2002 run period are plotted in Figure 1, **Figure 1**

showing the monthly average and standard deviation for each hourly bin along with corresponding NRL-MSIS model averages. The percentage variability, defined as standard deviation over the monthly average, is shown at the bottom of each panel.

T_{ex} maximizes in the afternoon between 1500–1600 LT, delayed by 3-4 hours from local noon (maximum solar zenith angle), and minimizes at 0600 LT before local sunrise. The observed T_{ex} monthly average agrees exceptionally well with MSIS during daytime hours (with deviation typically well less than 10K or 1%), while the NRL-MSIS model underestimates the observation by up to 50 K at night. The day-to-day variability is at the 5% level or 50–60 K, and changes little with local time, although T_{ex} itself changes substantially over 24 hours. The thermo-base temperature T_b is stable during the day, remaining at 340-350 K. However MSIS is close to or slightly more than one standard deviation away from the observed values in the afternoon. Overnight values are widely scattered, differing from MSIS predictions by up to 20%. However, this difference is within the day-to-day variability in the data. The inverse of the shape factor $1/s$ is on the order of 50 km during the day, and differences between the observation and MSIS model are particularly large at night (over 25 km). Variability in the observed $1/s$ is within 15-25%, and is small during the day. The large observational scatter at night for both T_b and $1/s$ is most likely due to weak ISR signals in the E-region as described earlier. However, further analysis of T_b and $1/s$ is beyond the scope of this paper which has a focus on T_{ex}.

We will first address variations at individual local times in Section 3, then in Section 4, we will discuss tidal components derived from the same dataset shown in Figure 1.

3.1. Solar irradiation effects

Solar geophysical conditions are known to be major sources of T_{ex} variability. To quantify these effects on thermospheric temperature, we take a straightforward approach by calculating the correlation coefficient between T_{ex} and geophysical indices. Figure 2 presents these correlation results as a function of local time, with shaded areas indicating areas where the null hypothesis of no correlation cannot be rejected (i.e.,no significant correlation exists). The shaded areas are estimated based on p-values >0.05.

Figure 2

In this section, we discuss the correlation between T_{ex} and the solar flux. F107 is a daily index for the solar radio flux at a wavelength of 10.7 cm and is widely used as a representation of overall solar activity level. In particular, it is a common solar EUV flux proxy for aeronomy studies. F107 is measured at local noon (2000UT) at Penticton, Canada, corresponding to 1500LT at Millstone Hill. Overall, there is a clear positive correlation between T_{ex} and F107. However, Figure 2 indicates that at 2000–2100 UT the correlation between T_{ex} and F107 maximizes, and after this time period (i.e. in the afternoon) the correlation is higher than before (in the morning). This morning-afternoon asymmetry can be associated partially with the 2000 UT observation time of F107, since T_{ex} for earlier times is therefore not directly related. The lowest correlation is at 0800UT (around 0300LT), 12 hours prior to the F107 data time. This also appears to be the time when T_{ex} is stable and correlated least significantly to magnetic activity index Dst (see Section 3.2).

To move beyond F107 proxy values, direct ultraviolet flux data are available from TIMED/SEE in situ measurements. The SEE instrument observes the Sun for about 3 minutes out of every orbit (97 minutes), producing 14–15 measurements per day. For

this study, we use SEE Space Weather data (http://lasp.colorado.edu/see/). These data contain 8 solar irradiance bands that are averaged over each 3-min solar observation with corrections applied for instrument degradation, 1-AU distance, and atmospheric absorption. The available SEE bands are coronal proxies [0.1–7 nm band, Fe XVI 33.5 nm line, and Mg IX 36.8 nm line], transition region proxies [27–34 nm band, He II 30.4 nm line, and H I 121.6 nm line], and chromospheric proxies [C II 133.5 nm line and the 145–165 nm band]. The FUV flux at the 121.6nm and 133.5nm lines and within 145–165nm band are also considered in this study, as their energy is deposited in the low thermosphere and thus may affect indirectly the upper thermosphere. Our correlation analysis indicates that T_{ex} is correlated insignificantly (falling well into the shaded area) to 0.1–7 nm band flux, so this band is excluded from further study in this section; influences of this band, including those from the variability of the emission, on tidal components will be discussed in Section 4.

In our correlation analysis, we use hourly T_{ex} data, with solar flux data matched to the nearest UT observation time from SEE. Initially, we examine EUV in the 27–34 nm band since, as discussed later this section, this flux tends to show maximum correlation with thermospheric temperature changes. Figure 2 indicates that correlation between 27–34 nm band EUV flux and T_{ex} is highest at 2000-2100 UT, when the diurnal variation of T_{ex} reaches maximum. During daylight hours, the correlation coefficient remains around 0.5 or up to 0.75. We also note that daytime correlation between T_{ex} and F107 is less robust than between T_{ex} and EUV at 27–34 nm. In fact, this is true also for 30.4 nm He II (transition region proxy), and 36.8 nm Mg IX (coronal proxy) bands, but definitely not true for the 0.1–7 nm band. Furthermore, better EUV data time resolution helps to

reduce the morning-afternoon correlation asymmetry seen with the F107 index. Some of these results for the high correlation between F107 and EUV agree with prior results, e.g., for EUV in the 27-34 nm band and HeII [Hedin, 1984].

We can further compare correlations for T_{ex} vs F107 and for T_{ex} vs EUV at 27–34 nm using T_{ex} residuals calculated for the entire period. The residuals are T_{ex} values after subtraction of dependencies on local time, season, and magnetic activity, and therefore should be dominated by solar flux variations. Dependencies are represented by a combination of diurnal, semidiurnal and terdiurnal harmonics (local time dependence), along with linear functions of the day number and Dst. Figure 3 shows these residuals (dots) as a function of either EUV (top panel) and F107 (bottom panel). Both EUV and F107 are shifted and normalized to be within -1 and 1 for easy comparison . The results show that T_{ex} residuals are more tightly clustered and have better linearity with EUV variations as compared to F107. The T_{ex} increase with F107 becomes saturated for high F107 values (~ 180).

Figure 3

3.1.1. Exospheric temperature relation as a function of solar flux band

T_{ex} response to solar flux depends on specific irradiation wavelength bands and emission lines. We sort all T_{ex} data for different days and local times into 24 hourly local time (converting to UT) bins. For each hourly bin, we calculate the correlation coefficient between T_{ex} and each band of EUV flux observations obtained at the nearest UT time. Then for each band we determine p_m, the maximum correlation among these 24 possible hourly correction coefficients (circles in the upper panel of Figure 4). We also determine p_a, the average correlation over the 10 highest correlation coefficients in the 24-hour period (dots in the upper panel of Figure 4). The results show that large correlations for both p_m

Figure 4

and p_a appear consistently in the 27–34, 30.4 and 36.8 nm bands, and low or no correlation occurs consistently at 133.5 nm. p_m at 121.5 nm is larger compared to p_m at other bands, but p_a at 121.5 nm is around the median value p_a of all other bands.

For each hourly UT time, the wavelength band f_{mx} with maximum correlation coefficient among all bands is shown by circles in the bottom panel of Figure 4. The band f_{mn} with minimum correlation is shown by dots in the same panel. We find that during 1200–2100 UT (0700–1600 LT, i.e., daytime hours), the highest T_{ex} - flux correlation appears in the 30.4 nm band, while at other times, the highest correlation appears at 27–34 nm. However, the lowest correlation between temperature and solar flux measured during the day is in the 145–165 nm band, while at other times the lowest correlation is at 133.5 nm. We conclude that among those solar flux bands that TIMED/SEE observes, the wavelength bands at 27–34 mm and 30.4 nm, proxies for the solar transition region, are most closely associated with T_{ex}. However, 133.5 nm and 145–165 nm bands, proxies for the chromosphere, are not strongly associated with T_{ex}. In particular, during the daytime, the correlation between the 145–165 nm band in the Schumann-Runge continuum and T_{ex} is the smallest among all bands concerned. This agrees with the general understanding that ultraviolet heating for wavelength region below Lyman β (102.6 nm) down to 8 nm is more important for the upper thermosphere, while the Schumann-Runge continuum heating may be more important for lower altitudes (e.g., around 120 km; see Banks and Kockarts [1973]).

Atmospheric absorption of solar irradiation energy by the neutrals is affected by the intensity of incoming solar flux and the photo-absorption cross-sections of neutral particles, both of which are wavelength dependent. The absorption is also dependent on

number density of specific neutral particles which are distributed as a function of height based on diffusive equilibrium in the thermosphere. Deposition of solar ultraviolet energy appears to reach a maximum at a specific altitude, where the product of the arriving solar flux intensity and neutral density maximizes. The height of this maximum depends on wavelength, because the photo-absorption cross-sections of different neutral species are wavelength dependent. As a result, EUV energy is generally absorbed the most in the upper thermosphere, soft X-ray energy is absorbed at $\sim$ 110 km, and FUV energy is absorbed in the lower thermosphere.

In the 8 bands/lines of solar emission observed by TIMED/SEE, the 27–34 nm, 30.4 nm, 33.5 nm and 36.8 nm bands correspond to the wavelengths at which photo-absorption, and photo-ionization cross-sections are high for O, N_2 and O_2, and therefore we expect these bands' solar flux effects on the ion density and neutral temperature to be effective. The absolute value of 27–34 nm flux is the highest, and we accordingly expect high correlation between T_{ex} and solar flux in this band. Of course, variability in the T_{ex} mean can be better correlated with other bands that have greater variability; this will be addressed in Section 4.5. The absolute value of 30.4 nm flux is the second highest, contributing 25–50% to the flux at 27–34 nm, and our results accordingly show a correlation between 27–34 nm and 30.4nm fluxes of 0.98 (compared to correlation coefficients of 0.94 for 27–34 nm vs 33.5 nm, and 0.93 for 27–34 nm vs 36.8 nm). We therefore expect equally high correlation between T_{ex} and 30.4 nm flux. Relative to the flux at 27–34 nm, the flux at 33.5 nm is $\sim$10%, and at 36.8 nm $\sim$4%. We note that even though the FUV fluxes at 121.5 nm and 133.5 nm are larger by a factor of several than flux at 27-34 nm, these FUV bands' effects on T_{ex} are much smaller, because at these wavelengths the primary neutral

species (e.g., O) in the thermosphere have generally small absorption cross-sections, while other neutral species (e.g., O_2) that absorb the FUV energy efficiently are abundant only at low thermospheric altitudes.

3.1.2. Time delay of T_{ex} responses to EUV flux variations

Earlier studies found that neutral density and T_{ex} are related to solar 10.7 cm flux for the previous day more than for the present day (see Roemer [1967] and Buonsanto and Pohlman [1998]). In fact, in the MSIS model, F107 for the previous day, rather than for the present day, is used to drive the model's variation with solar flux. It is unclear whether this delay is mostly due to the fact that F107 is measured at 2000 UT, i.e., at a later point in the UT day. However, Eastes et al. [2004] found that solar soft X-ray flux variations lead variations in neutral density by ∼1.5 days. The TIMED/SEE EUV data used here and ground-based thermospheric data have much better time resolutions than the daily F107 data, allowing us to examine more precisely (on the order of hours) the delay in T_{ex} compared to EUV dynamic variations. We show results in this section for the 27–34 nm band, with results comparable in other bands with high correlation coefficients.

We calculate correlation between T_{ex} at any given UT of the day and 27–34 nm flux observed at an earlier time, UT + t, where the lag time t (negative) is a variable. At a given lag time t, we compute the maximum correlation coefficient in each of 24 UT hourly bins, $p_m(t)$, and the average of the 10 highest correlation coefficients among these 24 hourly ones, $p_a(t)$. In Figure 5, we plot in the upper panel $p_m(t)$ (circles) and $p_a(t)$ (dots) as a function of lag time t, ranging between -110 ∼ 0 hours. We see that the maximum correlation $p_m(t)$ increases from 0.72 at $t \sim 0$ to 0.85 at $t \sim$ - 32–66 hours, then decreases

Figure 5

at longer time delays. This same trend can be found for $p_a(t)$, with highest correlation at a delay time of 1.33–2.75 days (32–66 hours).

The lag time of T_{ex} response to EUV flux is local time-dependent. $p_m(t)$ and $p_a(t)$ described in the previous paragraph are the correlation maxima and an approximation of the average correlation across the entire UT day. For further information, in Figure 5 (top panel), we also show the correlation curve for 2100 UT using cross symbols. The 2100 UT correlation turns out to be close to the curve of $p_m(t)$, and maximum correlation occurs at $t = \sim$ -54 hours of lag time. We estimate this maximum correlation lag time through a least-squared fit of the correlation (the crosses) to a parabolic curve (the dashed line). For each UT time bin, the lag time with maximum correlation can be determined using a similar least-squares fit approach, and the lag time for each UT hour is then shown in the bottom panel of Figure 5. We see that temperature EUV response delay time becomes increasingly longer as time progresses from morning hours (delay = 20–40 hours) to afternoon hours (delay = 40–60 hours).

The fact that T_{ex} responds to the 27–34 nm flux more slowly in the afternoon than in the morning may imply that thermospheric temperature solar flux preconditioning or "memory" is shorter in the morning than in the afternoon. The morning-afternoon difference is very common in the upper atmosphere. During its diurnal course as shown in Figure 1, T_{ex} has a minimum around 06-07LT near local sunrise, and increases gradually from morning through noon into afternoon, till 16LT when it reaches the daily maximum. Owing to different morning-afternoon atmospheric absorptions of solar UV energy arising from different morning-afternoon neutral densities, it is reasonable to expect that T_{ex} responses to solar flux variability in the afternoon can be quite different from those in

the morning. In fact, this scenario of local-time dependent thermospheric delay follows logically since in the morning hours, solar EUV heating rapidly builds up from a cool temperature background. Therefore, it dominates the thermal budget and provides a strong control on the temporal variation of thermospheric temperature. In the afternoon for a similar solar zenith angle and EUV intensity, neutral density and temperature are all close to the highest of the day [Mayr et al., 1973], then the time derivative $\partial T_n/\partial t \sim 0$ implying the thermospheric temperature responds only slowly to external heating. Apparently the local time dependency in the lag time mirrors a simple fact of the varying state of the non-stationary thermosphere throughout the day.

Zhang and Holt [2008] found the time delay of similar magnitude in ionospheric responses during another 30-day experiment at Millstone Hill in September 2005. The solar activity was at medium to low solar activity. The delay was found to be strongly height dependent: it occurred in the F2-region electron density and ion temperature, and mostly vanished in the E-region. It is likely that these ionospheric F2-region delays may be originated from that in neutral temperature (as demonstrated in this study), which affects the F-region ionospheric processes locally through neutral composition, ion-neutral energy exchange, plasma scale heights, and chemical reaction rates. A 0.8-1.3 day delay in equatorial TEC to soft X-ray irradiances was also noted by Wang et al. [2006] in a study using two-year long datasets between 1998-2000.

3.2. Other effects: magnetic activity and seasonal correlation

As stated earlier in Section 2, we have removed data with large negative Dst values before correlation analysis, and therefore this analysis excludes the significant effects of major magnetic activity on thermospheric circulation, composition and temperature. Al-

though not producing severe thermospheric/ionospheric variations, magnetic activity at weak to medium level exists much more often than these episodic but dramatic magnetic events, and therefore it provides an important source of upper atmospheric variability, with effects visible in our analysis. In general, T_{ex} tends to increase as ap increases or Dst drops, as shown in Figure 2. However, correlation between T_{ex} and ap is for the most part lower than that between T_{ex} and Dst. T_{ex} and Dst correlation is slightly lower during the day (1100–2400 UT) and slightly higher at night. The highest correlation values for T_{ex}-Dst occur around pre-midnight at 0300–0500 UT (2200–2400LT), and the lowest occur around near 0800UT (0300LT). Figure 6 plots correlation between T_{ex} and Dst at 1530 LT and 0600 LT, where T_{ex} is calculated as the residual of removing EUV effects, defined as $T - b - d \times D - c_1 \times F - c_2 \times F^2$, where T is the original exospheric temperature data for the 30-day time period, D day number, F the corresponding SEE EUV data at 27–34 nm band as a solar flux proxy, and b, c_1 and c_2 are obtained from a least squared fit based on this 30-day dataset. After removing EUV effects, T_{ex} and Dst correlation can be as high as -0.56 at 0600 hour LT, and negative correlation is also clear at 1530 hour LT when the diurnal thermosphere temperature maximum is reached. This pronounced correlation occurs consistently throughout the entire range of Dst values, including Dst values associated with low magnetic activity (more positive values). We conclude from this T_{ex} dependence on Dst that low magnetic activity also contributes to day-to-day variability in T_{ex} over Millstone Hill.

Figure 6

Similar to solar flux effects, the upper atmosphere responds to magnetic activity with a time delay, depending on the type of disturbances and atmospheric conditions. At Millstone Hill , T_i responses were found [Zhang and Holt, 2008]to be delayed by 6-9 h

from the 3-hourly ap index, and Ne responses are delayed by 0-3 h below the F2 peak, and 9-12 h above the peak. Therefore we might expect a time delay of a few hours in the thermospheric temperature, and this delay is much shorter than that associated with solar UV flux. In general, thermospheric variability driven by magnetic activity is another complicated subject and is beyond the primary scope of this study.

Seasonal dependence within the 30-day period is very significant, and produces consistently high correlations for each hour of the day. Since the Millstone Hill experiment took place in October 2002 toward winter solstice from the fall equinox, solar zenith angle increases for the same local time each day, and T_{ex} decreases with the day number (also seen in Figure 2). This implies that seasonal trends in the daily T_{ex} maximum at 1600 LT (2100UT) are the strongest seen over a full UT day.

4. Variability in T_{ex} tidal components

The analysis above has discussed variability at given local times. In this section, we investigate day-to-day variability in the tidal components of thermospheric temperature, and quantitatively examine effects of EUV and magnetic activity. For this study, we use a tidal decomposition into daily mean, diurnal and semidiurnal components.

4.1. EUV effects on T_{ex} tidal components

In analysis of EUV effects on T_{ex} tidal components, we use daily averaged EUV flux measured by TIMED/SEE in the same bands as above. The correlation coefficients between each of the three tidal components of thermospheric temperature (daily mean, diurnal, semidiurnal) and solar EUV flux at each band are shown in Figure 7 where the coefficients with and without a 2-day time lag in responses to EUV flux are also given.

Figure 7

The correlation between the T_{ex} daily mean and all the EUV bands examined (except for the X-ray proxy at 0.1–7 nm) is very strong, with correlation coefficients generally above 0.6. Furthermore, the two-day delay values show a large increase in correlation for short wavelength bands (27–34, 30.4, 33.5, and 36.6 nm, except for 0.1–7 nm), but not for long wavelength bands.

The T_{ex} diurnal amplitude (day-night difference) is weakly correlated, or not correlated at all, to EUV flux. This implies that the day-night difference in T_{ex} responses to EUV is not significant, even though the solar EUV flux disappears at night. This is another example of the thermospheric solar preconditioning or "memory" effect. We also find that the 2-day time delay effect is much stronger at long wavelengths with positive and significant correlation (121.5, 133.5, and 145–165 nm) as compared to short wavelengths (27–34, 30.4, 33.5, and 36.6 nm). This may indicate that the delayed response of exospheric temperature, in particular its diurnal amplitude, is related to heating in the low thermosphere. Also interestingly, the delay effect is particularly significant at 0.1-7 nm where the correlation is merely 0.2 (and not statistically significant) if the delay is not considered, but is 0.6 if the delay is considered.

The T_{ex} semidiurnal amplitude is also weakly correlated to the EUV flux. The 2-day time delay effect can be seen clearly in a resulting larger negative correlation (or smaller positive correlation) value. Once again, the 0.1–7 nm band contains unusual correlation to T_{ex} that is very different from other bands. For this band, the time delay effect is so significant that the correlation is improved from -0.2 (when the delay is not included) to -0.6 (when it is included).

The direct impact of the soft X-ray flux (from the same day) on T_{ex} diurnal and semidiurnal amplitudes is in general weak, and the correlation with the solar X-ray from 2 days earlier is high. Very strong soft X-ray events have the potential to impact deep into the lower atmosphere, and then the deposited energy may propagate to the upper thermosphere with a lag time. However, for the data we are examining, the intensity and frequency of such X-ray events do not appear to be substantial, as the percentage variability (standard deviation/mean) is only $\sim 10\%$, and therefore their role in producing delayed thermospheric variations should not be overestimated. On the other hand, these observations of delayed thermospheric response may be associated with some processes accompanying solar X-ray changes, such as high energy particle flows taking more than 1 day to reach Earth's upper atmosphere with the effect of different responses of T_{ex} during different times. We conclude that time-shifted solar X-ray (0.1–7 nm) data may be used as another proxy to account for some thermospheric temperature variations caused by solar-geophysical disturbances. (In fact, results in subsequent sections do show some similarity between solar flux effects and Dst effects.)

Discussions on time delay so far have addressed effects of individual prior times (days), and in particular, the question about which prior time is most strongly correlated to T_{ex}. However, if solar flux history is important, solar flux effects can be accumulated over time with different weighting on different days. We further examine this possibility by using a composite solar flux proxy E_w to consider integrated influences on T_{ex} daily means. We define $E_w = c_0E_0 + c_{-1}E_{-1} + c_{-2}E_{-2} + c_{-3}E_{-3}$, where E_0, E_{-1}, E_{-2} and E_{-3} are solar UV flux (at a given wavelength or band) for the current day, one, two and three days prior to the current day when a particular T_{ex} daily mean is taken. Coefficients c_0, c_{-1}, c_{-2} and

c_{-3} are determined by varying E_w (through varying these coefficients) and searching for the largest correlation between daily E_w and daily mean T_{ex}. These different coefficients obtained with the 30-day datasets, listed in Table 1, may represent relative importance of the solar flux on individual days to overall solar irradiation conditions that correlate to daily mean T_{ex}. Results show that the significance of the 2-day delay becomes less important compared to that of the 3-day delay with increasing solar irradiation wavelength (from EUV to FUV), and the current day flux remains a significant factor for soft X-ray and FUV bands. As a result of using the weighted contributions from different days, the correlation between E_w and daily mean T_{ex} (squares in Figure 7) is normally higher than using the solar flux from an individual day.

4.2. T_{ex} daily mean

The observed T_{ex} daily mean peaks at day 288 then drops to a minimum 8 days later (cf. solid line the upper panel of Figure 8). This variation is mostly due to solar EUV changes. In fact, a simple EUV-based empirical model containing a linear EUV term and a quadratic EUV term in the form $f_0 + f_1 \times F + f_2 \times F^2$ can reproduce the observed daily mean rather well (triangles in the top panel). In the model, the EUV flux F is the daily average flux at 27–34 nm with a 2-day time delay considered (cf. previous section) and f_0, f_1 and f_2 are obtained through a least squared fit. However, the daily mean is not very sensitive to Dst. A similar polynomial model using Dst instead as an independent variable does not generally reproduce absolute values of the daily mean well. However, the relative fluctuations in daily mean between days 300–305 are in fact well represented by a Dst only empirical model, while they are not well represented by the EUV only empirical model. We therefore find that an empirical model which combines these EUV and Dst

Figure 8

terms and further includes a seasonal variation term can almost perfectly reproduce T_{ex} observations (cf. line and dots).

To quantify relative contributions of these various factors on variability in the T_{ex} daily mean, we derive the percentage variability in both the observational data and in the model regression data. This percentage variability is defined as the standard deviation from the average divided by the average, computed over the entire 30 day observational period. We can estimate relative contributions by calculating the standard deviation above the average in the model regression data over the standard deviation in the observational data. The results are shown in Figure 9, with observed T_{ex} percentage variability of 4–5% (upper panel). EUV flux variability alone (i.e., variability generated by the above-mentioned EUV only empirical model) can account for 90% of the observed variability, while variability in Dst alone (i.e., variability generated by the above-mentioned Dst only empirical model) produces 45% of the observed variability. We find that the combined effects of EUV, Dst and seasonal changes (as given by an empirical model with EUV and Dst terms) can explain nearly all of the observed variability (bottom panel).

Figure 9

4.3. T_{ex} diurnal amplitude

We apply the same analysis technique as in the previous section for the T_{ex} daily mean to the T_{ex} diurnal and semidiurnal amplitudes. The diurnal amplitude (the middle panel in Figure 8) is in the range between 100–140 K, approximately 10% of the daily mean, and fluctuates more than the daily mean. The large and rapid fluctuations between days 295 and 305 appear to be highly correlated with EUV flux at 0.1–7 nm band from two days in advance, and accordingly the EUV-based empirical model of T_{ex} based on such flux values captures these fluctuations well. The Dst-based empirical model does generate

some fluctuations with a major drop from day 296 to 299, similar to observations, but their phases do not always agree with observations. Overall, the T_{ex} diurnal amplitude in the empirical model combining all the three factors (EUV flux, Dst and season) again reproduces those main fluctuations in the data.

The observed variability in T_{ex} diurnal amplitude is 12% (Figure 9). The EUV-based empirical model generated variability is 9% and the Dst generated variability is 6%. Finally, the T_{ex} empirical model including EUV, Dst and seasonal changes generates 10% variability, or 80% of the total observed variability in the diurnal amplitude. We can therefore quantify the remaining 20% of variability seen in diurnal amplitude observations as due to other controlling factors beyond those considered here. These may include various wave activities due to vertical coupling processes from the lower atmosphere into thermosphere, residual magnetic activity effects, additional ionospheric energy inputs to the thermosphere, and possibly measurement uncertainty.

4.4. T_{ex} semidiurnal amplitude

The T_{ex} semidiurnal amplitude (bottom panel of Figure 8) is about 1/3 of the T_{ex} diurnal amplitude (See Figure 8), and fluctuates between 20–50 K, with a day-to-day variability of 31%. Both EUV-based (based on the EUV flux at 0.1–7 nm band for 2 days in advance) and Dst-based empirical models can capture some of the fluctuations, and the combined T_{ex} empirical model for the semidiurnal component generates 78% of the total observed variability (Figure 9), once again with the remaining 22% of variability due to other factors besides EUV, Dst, and seasonal effects. For semidiurnal variations, Dst control is now as significant as in the EUV flux. We note with interest that both in T_{ex} diurnal and semidiurnal amplitudes, there are some obvious 3–5 day fluctuations that

seem to be associated with Dst changes, while for the T_{ex} daily mean, Dst effects are less important and EUV flux effects are dominant.

4.5. Day-to-day fluctuations

Our correlation analysis has addressed the direct relationship between T_{ex} and EUV flux, both of which experience strong day-to-day variability. A further question is how the day-to-day fluctuation in T_{ex} is correlated to that in EUV. Here, fluctuations are defined as deviation of daily values from means or expected values. Hedin [1984] indicated that fluctuations of EUV and neutral density, obtained with deviation of daily values from the slow-varying 81-day running averages, show correlation that varies with wavelength of the solar irradiation flux, being high with EUV bands of significantly low total energy. To examine this type of day-to-day variability using our 30-day observations, we consider daily fluctuations relative to the 3-day running means. Figure 10 is similar to Figure 7 (top) but here we use solar flux fluctuations (residuals of daily means from its 3-day running means), as well as the T_{ex} daily fluctuations defined in the same way as solar flux fluctuations. Results show that the there still exists very strong correlation between the main EUV bands and the time-delayed T_{ex}. For instance, correlation with the 36.8 nm flux is among the strongest; the correlation appears low at FUV bands/lines and the soft X-ray band. The delay time is 2 days for the EUV flux, and 3 days for the FUV flux.

Figure 10

These results confirm that during this 30-day experiment, short-term variability in the EUV flux is very likely the primary driver for T_{ex} short-term variability. They are also consistent with Hedin [1984] indicating that EUV fluxes at wavelengths slightly longer than 30.4 nm are more important to the short-term variability in the exospheric temperature than the 30.4 nm emission, and that the fluxes at wavelengths shorter than 30.4

nm are also more important in producing the short term variability. Although the 30.4 nm emission contains significantly more energy, it varies less and therefore produces less thermospheric variations.

Eastes et al. [2004] indicated that variability (relative to the 81-day means) in the soft X-ray flux has much better correlation with that in neutral density than does the F107 variability. However, we show very low correlation between variabilities (relative to the 3-day mean) in the 0.1-7 nm emission and in the T_{ex} diurnal mean. It appears that the short-term (3 days) and long-term (81 days) variability in this 0.1-7 nm emissions has different influences on the corresponding thermospheric variability. The most significant influence of the 0.1-7 nm emission that was found in this work (see the last two sections) is on the amplitudes in diurnal and semidiurnal tides with a 2-day lag.

5. Summary and conclusion

We have quantified thermospheric temperature variability in response to solar and geomagnetic effects using a 30-day ISR observation at Millstone Hill during October 2002. We analyzed exospheric temperature T_{ex}, derived from the radar observation, to examine day-to-day variability at fixed local times and also in the temperature daily mean and the two tidal components (diurnal and semidiurnal amplitudes). The driving factors considered responsible for the observed variability include solar EUV flux, magnetic activity, and season, and these relationships have been explored quantitatively. The solar EUV flux used is from the TIMED/SEE space weather product, allowing for detailed studies of the correlation between EUV variability and T_{ex} variability, EUV band dependence, and time delay of thermospheric solar preconditioning response (thermospheric "memory"). Our main findings can be summarized as follows:

583 (1) During the day, correlation between T_{ex} and EUV flux (except for at the 0.1–7 nm
584 band) is much higher than that between T_{ex} and F107. We conclude that EUV data,
585 as compared to daily F107, is essential to a quantitative understanding of thermospheric
586 temperature T_{ex} day-to-day variability.

587 (2) There is a ∼20–60 hour delay in T_{ex} response to solar EUV flux. The delay time is
588 shorter in the morning when solar heating changes most rapidly in the upper atmosphere,
589 and longer in the afternoon and at night.

590 (3) T_{ex} is most sensitive to the EUV flux at wavelengths of 27–34 nm and 30.4 nm.
591 The short-term variability in T_{ex}, however, is better correlated with that in wavelengths
592 of 27–34 nm than at wavelength 30.4 nm, consistent with Hedin [1984]. T_{ex} is relatively
593 less sensitive to the flux at 133.5 nm and 145–165 nm.

594 (4) Magnetic activity control of T_{ex} tends to be weaker during the day and stronger
595 at night. We attribute this to the nighttime absence of solar ultraviolet irradiation,
596 constituting the majority of upper atmospheric heat input.

597 (5) The daily mean of T_{ex} strongly depends on EUV flux. An empirical model driven
598 only by the EUV flux at 27–34 nm with a 2-day time delay can generate 90% of the
599 observed variability in the daily mean. The two-day delay effect is less significant for
600 EUV fluxes at longer wavelengths (121.5, 133.5, and 145–165 nm).

601 (6) The diurnal T_{ex} amplitude is not sensitive to solar EUV flux unless a 2-day time delay
602 is applied for long wavelengths, implying similar daytime and nighttime T_{ex} responses,
603 even though significant solar irradiance is absent at night. Additionally, the 0.1–7 nm
604 band EUV flux is clearly positively correlated to diurnal T_{ex} amplitude with a two-day

time delay, implying oppose daytime and nighttime responses. Effects of the time delay for other than 2 days are weaker.

(7) Semidiurnal T_{ex} amplitude variability is negatively correlated only with the 0.1–7 nm band with a 2-day time delay. With a delay time other than 2 days the correlations are much weaker.

(8) Magnetic activity as represented by the Dst index is, across T_{ex} daily mean, diurnal and semidiurnal components, most important for the semidiurnal amplitude and least important for the the daily mean. This behavior is similar to T_{ex} soft X-ray response at 0.1-7 nm band with a 2-day delay, implying that there might be a direct connection between magnetic activity and time-shifted solar data.

This study provides a detailed and quantified insight into EUV flux effects on thermospheric temperature variability at midlatitudes (or sub-auroral latitudes during disturbances). However, some of those findings listed above need to be fully explained with the help of theoretical models, in particular, the delayed T_{ex} response to EUV flux and the associated thermospheric solar preconditioning or "memory". These delayed responses appear to be wavelength band dependent, being significant in the daily mean for the 27-34 nm band, in the diurnal and semidiurnal amplitudes for soft X-ray flux at 0.1–7 nm, and in the diurnal amplitude for longer wavelengths. Further studies focusing on different levels of solar activity and different seasons, and combining theoretical modeling with observational data analysis, are needed to better understand day-to-day variability in the thermosphere.

Acknowledgments. We thank the members of the Atmospheric Sciences Group at MIT Haystack Observatory for assembling and maintaining Millstone Hill observations

628 and the Madrigal distributed database. SRZ is indebted to Prof. William L. Oliver
629 for making available the thermospheric calculation program which forms the main ba-
630 sis of deriving neutral temperatures from ISR measurements as presented in this work.
631 Observations and analysis at Millstone Hill are supported by a cooperative agreement
632 between the National Science Foundation and the Massachusetts Institute of Technol-
633 ogy (AGS-1242204). This work is also supported by the NSF award AGS-1042569 to
634 MIT. SEE space weather data products have been obtained from the SEE web site at
635 http://lasp.colorado.edu/see/. The TIMED spacecraft was developed by the Johns Hop-
636 kins University Applied Physics Laboratory. The TIMED mission, including the SEE
637 instrument, is sponsored by NASA's Office of Space Science.

References

638 Alcaydé, D., J. Fontanari and P. Bauer (1982), High latitude neutral atmosphere tem-
639 perature and concentration measurements from the first EISCAT incoherent scatter
640 observations, *Ann. Geophys.,* 38, 473-479.

641 Altadill, D., and E. M. Apostolov, Vertical propagating signatures of wave-type oscilla-
642 tions (2- and 6.5-days) in the ionosphere obtained from electron-density profiles (2001),
643 *J. Atmos. Sol. Terr. Phys.,* 63, 823-834.

644 Banks, P. M., and G. Kockarts (1973), Aeronomy, Part B, *Academic Press*, P.19, New
645 York and London.

646 Bauer P., P. Waldteufel and D. Alcaydé(1970), Diurnal variations of the atomic oxygen
647 density determined from incoherent scatter measurements in the ionospheric F-region,
648 *J. Geophys. Res.,* 75, 4825-4832.

649 Buonsanto, M. J., and L. M. Pohlman (1998), Climatology of neutral exospheric temper-
650 ature above Millstone Hill, *J. Geophys. Res.,* 103 , 23381-23392.
651 Eastes, R., S. Bailey, B. Bowman, F. Marcos, J. Wise, and T. Woods (2004), The corre-
652 spondence between thermospheric neutral densities and broadband measurements of the
653 total solar soft X-ray flux, *Geophys. Res. Lett.,* 31, L19804, doi:10.1029/2004GL020801.
654 Forbes, J. M., S. E. Palo, X. Zhang (2000), Variability of the ionosphere, *J. Atmos. Sol.*
655 *Terr. Phys.,* 62, 685-693.
656 Forbes, J. M., and X. Zhang (1997), Quasi 2-day oscillation of the ionosphere: a statistical
657 study, *J. Atmos. Sol. Terr. Phys.,* 59, 1025-1034, 1997.
658 Goncharenko, L. P., J. L. Chau, H.-L. Liu, and A. J. Coster (2010), Unexpected con-
659 nections between the stratosphere and ionosphere, *Geophys. Res. Lett.,* 37, L10101,
660 doi:10.1029/2010GL043125.
661 Hagan, M. E., and W. L. Oliver (1985), Solar cycle variability of exospheric temperature
662 at Millstone Hill between 1970 and 1980, *J. Geophys. Res.,* 90, 12265-12270.
663 Hedin, A. E. (1984), Correlations between thermospheric density and temperature, solar
664 EUV flux and 10.7-cm flux variations, *J. Geophys. Res.,* 89, 9828-9834.
665 Hedin, A.E. (1987), MSIS 86 thermospheric model, *J. Geophys. Res.,* 92, 4649-4662.
666 Laštovička, J. (2006), Forcing of the ionosphere by waves from below, *J. Atmos. Sol. Terr.*
667 *Phys.,* 68, 479-497.
668 Jakowski, N., B. Fichtelmann and A. Jungstand (1991), Solar activity control of iono-
669 spheric and thermospheric processes, *J. Atmos. Terr. Phys.,* 51, 1125-1130.
670 Litvin, A., W. L. Oliver, J. M. Picone, and M. J. Buonsanto (2000), The upper atmosphere
671 during the 5-11 June 1991 magnetic storm, *J. Geophys. Res.,* 105 , 12789-12796.

672 Mayr, H. G., I. Harris, and H. Volland (1973), Theory of the phase anomaly in the
673 thermosphere, *J. Geophys. Res.,* 78(31), 74807489, doi:10.1029/JA078i031p07480.
674 Mendillo, M., H. Rishbeth, R. G. Roble, and J. Wroten (2002), Modelling F2-layer seasonal
675 trends and day-to-day variability driven by coupling with the lower atmosphere, *J.*
676 *Atmos. Sol. Terr. Phys.,* 64, 1911-1931.
677 Mikhailov, A. V., and J. Lilensten (2004), A revised method to extract thermospheric
678 parameters from incoherent scatter observations, Ann. Geophys., 47(N2/3), 985-1008.
679 Moore, L., M. Mendillo, C. Martinis, and S. Bailey (2006), Day-to-day variability of the
680 E layer, J. Geophys. Res., 111, A06307, doi:10.1029/2005JA011448.
681 Nicolls, M. J., N. Aponte, S. A. González, M. P. Sulzer, and W. L. Oliver (2006), Daytime
682 F region ion energy balance at Arecibo for moderate to high solar flux conditions, *J.*
683 *Geophys. Res.,* 111, A10307, doi:10.1029/2006JA011664.
684 Oliver, W. L. (1979), Incoherent scatter radar studies of the daytime middle thermosphere,
685 *Ann. Geophys.,* 35, (3), 121-139.
686 Oliver, W. L. (1997), Hot oxygen and the ion energy budget, *J. Geophys. Res.,* 102,
687 2503-2511.
688 Oliver, W. L., and K. Glotfelty (1996), O^+-O collision cross section and long-term F
689 region O density variations deduced from the ionospheric energy budget, *J. Geophys.*
690 *Res.,* 101, 21769-21784.
691 Oliver, W. L.; Salah, Joseph E. (1988), The global thermospheric mapping study, *J.*
692 *Geophys. Res.,* 93, 4039-4059.
693 Picone, J. M., A. E. Hedin, D. P. Drob, and A. C. Aikin (2002), NRLMSISE-00 empirical
694 model of the atmosphere: Statistical comparisons and scientific issues, *J. Geophys. Res.,*

107, 1468, doi:10.1029/2002JA009430.

Roemer, M. (1967), Geomagnetic activity effect and 27-day variation: Responses time of the thermosphere and lower exosphere, *Space Res.*, VII, 1091-1099.

Rishbeth, H., Day-to-day ionospheric variations in a period of high solar activity (1993), *J. Atmos. Terr. Phys., 55*, 165-171.

Rishbeth, H. (2006), F-region links with the lower atmosphere? *J. Atmos. Sol. Terr. Phys.,* 68, 469-478.

Rishbeth, H. (2007), Thermospheric targets, Eos Trans. AGU, 88(17), 189, doi:10.1029/2007EO170002

Rishbeth, H., and M. Mendillo (2001), Patterns of F2-layer variability, *J. Atmos. Sol. Terr. Phys.,* 63, 1661-1680.

Salah, J. E., and J. V. Evans (1973), Measurements of thermospheric temperatures by incoherent scatter radar, Space Research, 13 , 267.

Sugiura, M., (1964), Hourly values of equatorial Dst for the IGY, Ann. Int. Geophys. Year, 35, 9, Pergamon Press, Oxford.

Wang, X., R. Eastes, S. Weichecki Vergara, S. Bailey, C. Valladares, and T. Woods (2006), On the short-term relationship between solar soft X-ray irradiances and equatorial total electron content (TEC), *J. Geophys. Res.,* 111, A10S15, doi:10.1029/2005JA011488.

Wanliss, J. A., and K. M. Showalter (2006), High-resolution global storm index: Dst versus SYM-H, *J. Geophys. Res.,* 111, A02202, doi:10.1029/2005JA011034.

Zhang, S.-R. and J. M. Holt (2008), Ionospheric variability from an incoherent scatter radar long-duration experiment at Millstone Hill, J. Geophys. Res., 113, A03310, doi:10.1029/2007JA012639.

718 Zhang, S.-R., J. M. Holt, P. J. Erickson, F. D. Lind, J. C. Foster, A. P. van Eyken,
719 Y. Zhang, L. J. Paxton, W. C. Rideout, L. P. Goncharenko, and G. R. Campbell
720 (2005), October 2002 30-day Incoherent Scatter Radar Experiments at Millstone Hill
721 and Svalbard and Simultaneous GUVI/TIMED Observations, *Geophys. Res. Lett.,* 32,
722 L01108, doi:10.1029/2004GL020732.

723 Zhang, S.-R. and J. M. Holt (2008), Ionospheric climatology and variability from long-term
724 and multiple incoherent scatter radar observations: variability, Annales Geophysicae,
725 *Ann. Geophys.,* 26, 1525-1537, doi:10.5194/angeo-26-1525-2008

726 Zhang, S.-R., W. L. Oliver, S. Fukao, and S. Kawamura (2001), Extraction of solar and
727 thermospheric information from the ionospheric electron density profile, J. Geophys.
728 Res., 106(A7), 12821-12836, doi:10.1029/2000JA000403.

729 Zhang, S.-R., W. L. Oliver, J. M. Holt, and S. Fukao (2003), Ionospheric data assimilation:
730 Comparison of extracted parameters using full density profiles and key parameters, J.
731 Geophys. Res., 108, 1131, doi:10.1029/2002JA009521, A3.

732 Table 1. Composed EUV index Ew with weighted contribution from prior days.

733

nm	c_0(0d)	c_{-1}(-1d)	c_{-2}(-2d)	c_{-3}(-3d)
0.1-7	0.77	0.13	0.05	0.05
27-34	0.05	0.05	0.85	0.00
30.4	0.05	0.05	0.77	0.13
33.5	0.03	0.03	0.47	0.47
36.8	0.32	0.04	0.11	0.53
121.5	0.53	0.03	0.03	0.41
133.5	0.53	0.03	0.03	0.41
145-165	0.56	0.04	0.04	0.36
$Ew = c_0E_0 + c_{-1}E_{-1} + c_{-2}E_{-2} + c_{-3}E_{-3}$				

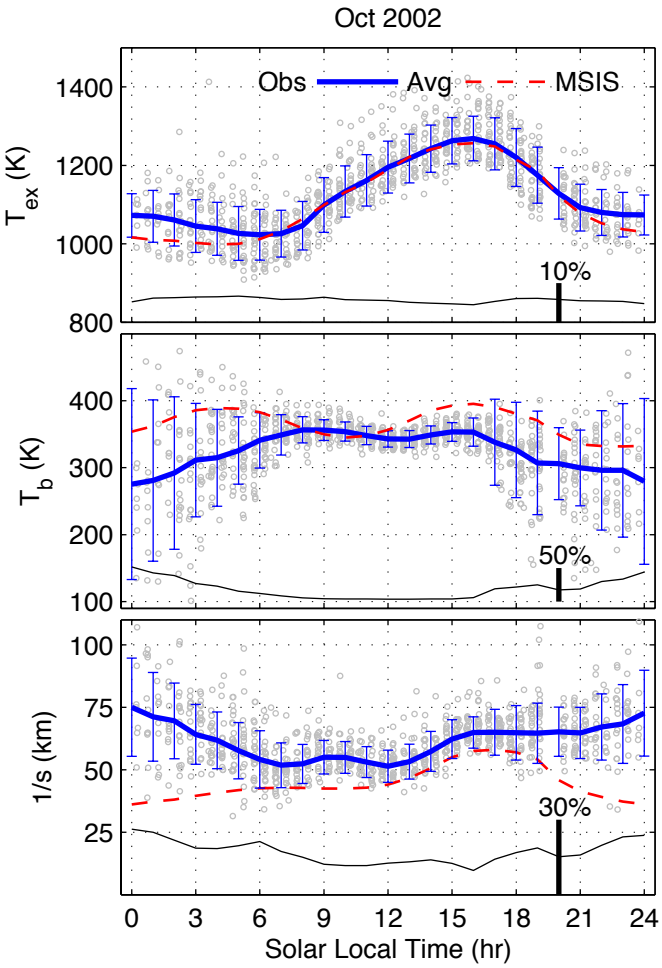

Figure 1. Diurnal variations of thermospheric temperature parameters: exosphere temperature T_{ex}, base temperature T_b, and the inverse of shape factor $1/s$ (see text), as well as their day-to-day variability. The gray dots are data points, the blue line is the hourly average of the month with error bar representing the standard deviation, and the dashed line shows MSIS model averages. The dark thin line near the bottom of each panel shows the percentage variability; a vertical thick line on the dark thin line provides the scale for the corresponding percentage variability marked above the vertical line.

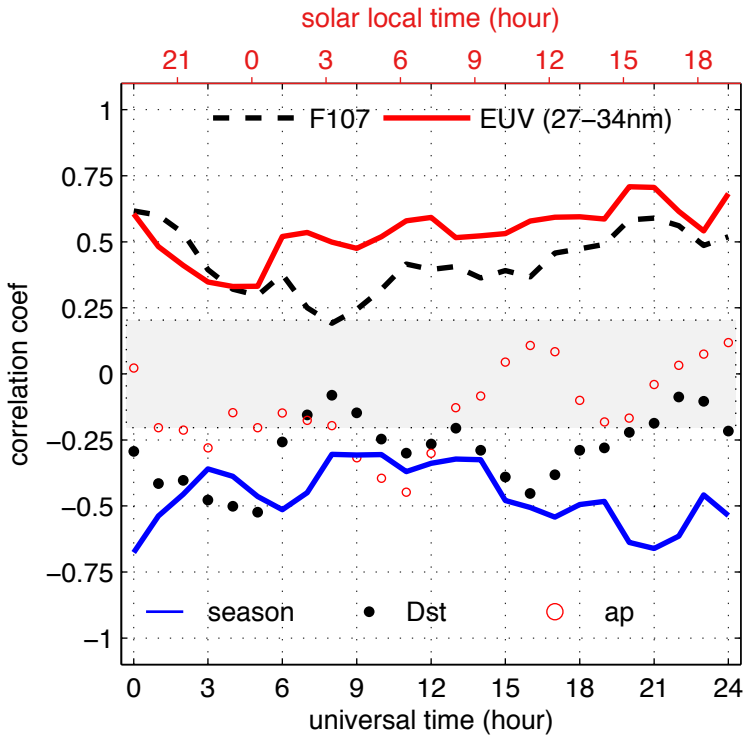

Figure 2. Diurnal variations of exospheric temperature correlation with solar-geophysical parameters. These parameters include solar irradiation indices of daily F107 and EUV flux at 27–34 nm observed with TIMED/SEE, along with magnetic activity indices of 3-hourly ap (converted to negative values, -ap, to place the correlation curve on the negative side for easy comparison with the Dst curve) and hourly Dst. Seasonal dependency of T_{ex} is expressed as its correlation to the day number. The shaded area represents regions where p-values$>$ 0.05 (typically 66 data samples for an hourly window of 30 individual days that pass the Dst filters) indicating a failure to reject the null hypothesis of no correlation. UT - SLT = 4.76 hr at Millstone Hill.

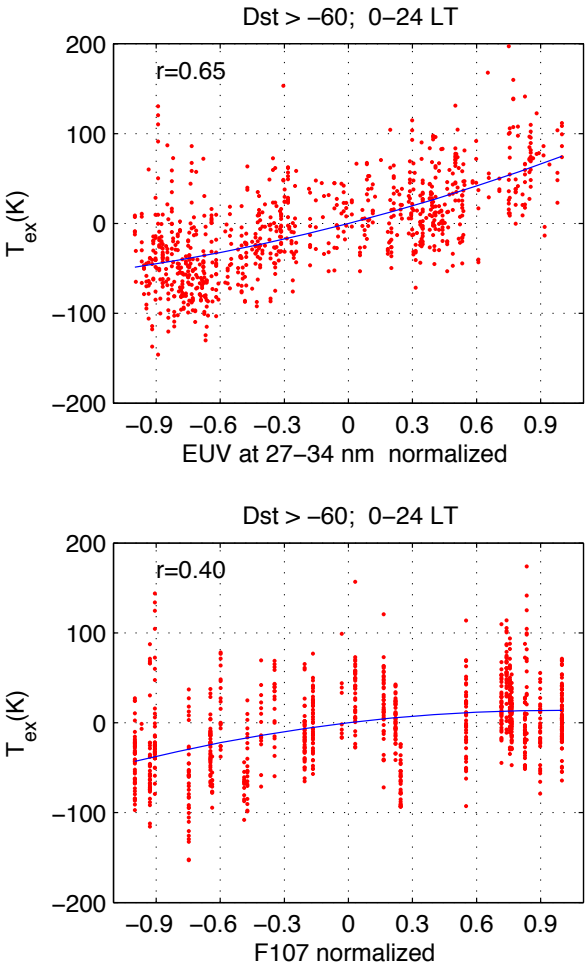

Figure 3. Correlations between T_{ex} residuals and F107 (bottom), and between T_{ex} residuals and EUV flux at 27-34 nm (top). The residuals are T_{ex} data after subtraction of dependencies on local time, season, and magnetic activity, and therefore should be dominated by solar flux variations. Dependencies are represented by a combination of diurnal, semidiurnal and terdiurnal harmonics (local time dependence), along with linear functions of the day number and Dst, and are determined through least squares fitting. The T_{ex} data are subtracted by regression data representing those dependencies, yielding T_{ex} residuals. Both EUV and F107 are shifted and normalized to be within -1 and 1 for easy comparison. Blue curves are fitting results with parabolic functions.

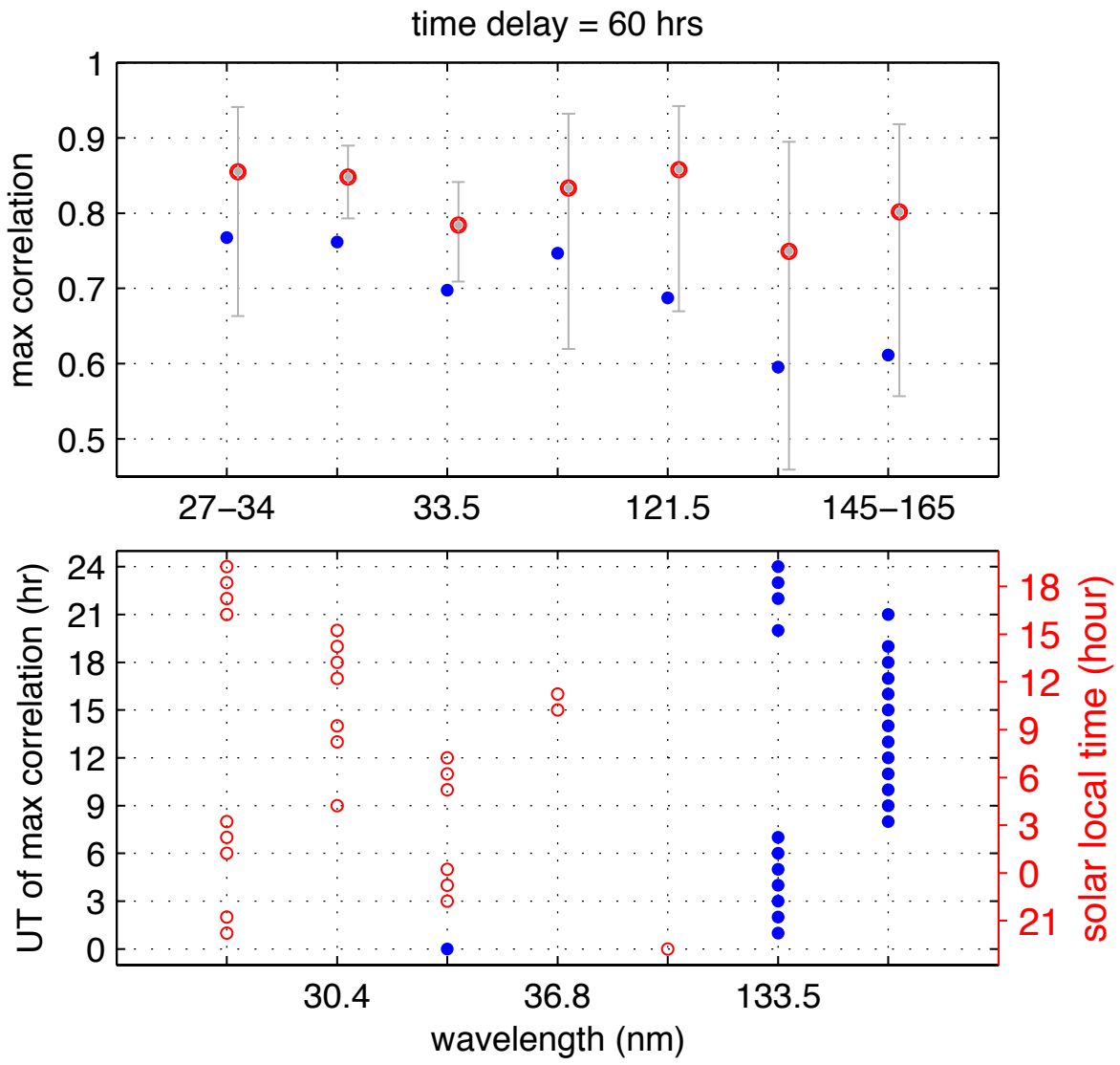

Figure 4. Correlation between T_{ex} and EUV flux at different wavelengths. Top panel: highest correlation (circles) and the average of the first 10 highest correlation (dots) for the 24 hourly time bins as a function of wavelength. The vertical bars indicate 95% confidence intervals. Bottom panel: the wavelength for each UT hour when highest correlation (circles) and lowest correlation (dots) occur.

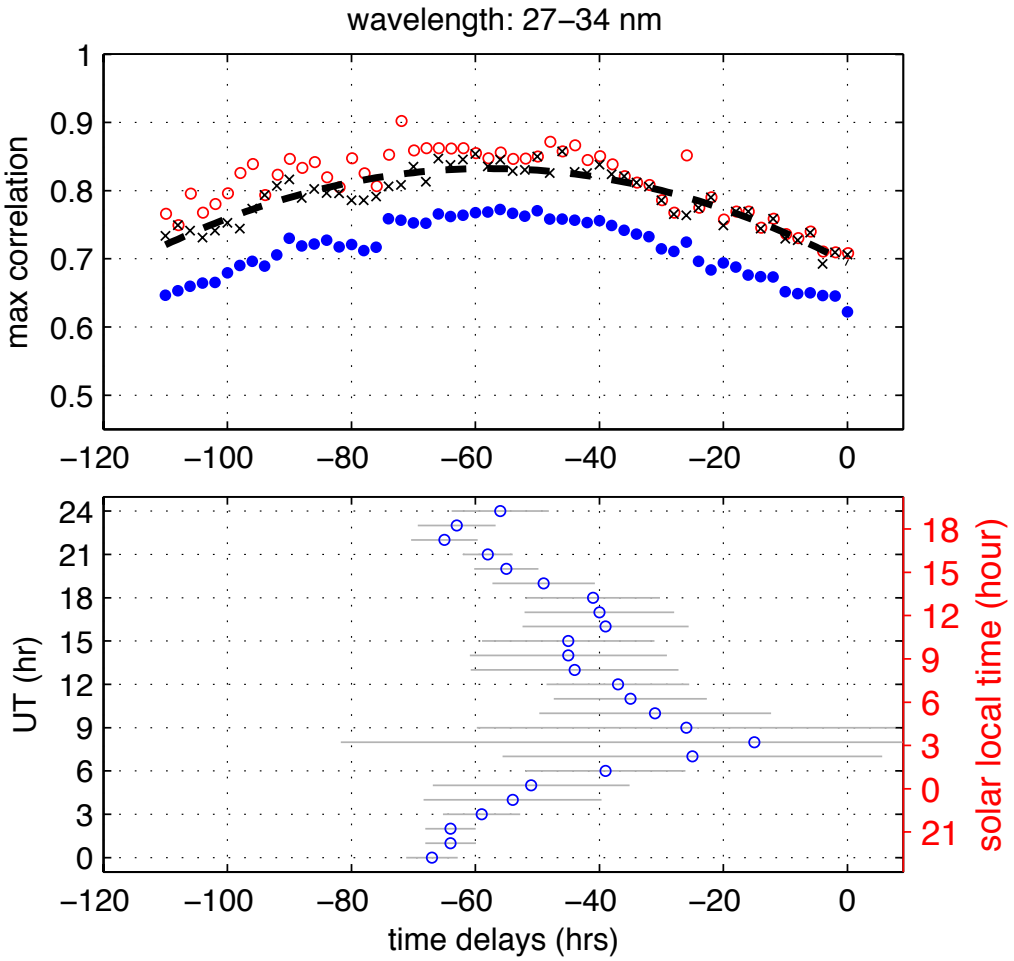

Figure 5. Time delay of T_{ex} response to EUV flux at different wavelengths. The plots show correlation between T_{ex} and the EUV at a given band (27-34 nm) with a variable delay from 0 (now) to 110 hours before (i.e., delay time) with 2-hour resolution. Top panel: highest correlation (red circles) of the day and the average of the first 10 highest correlation (blue dots) in the 24 hourly time bins as a function of delay hours; also shown is the correlation for 2100 UT (black crosses) and a parabolic fit (dashed line). Bottom panel: delay values in hours for each UT hour at which maximum correlation is obtained. The largest correlation is determined from a least-squared fit of the correlation curve to a parabolic curve at a given UT time, as indicated by the crosses and the dash line in the upper panel. The horizontal bars provide standard deviation estimation based on least-squares fitting residuals and the parabolic model function.

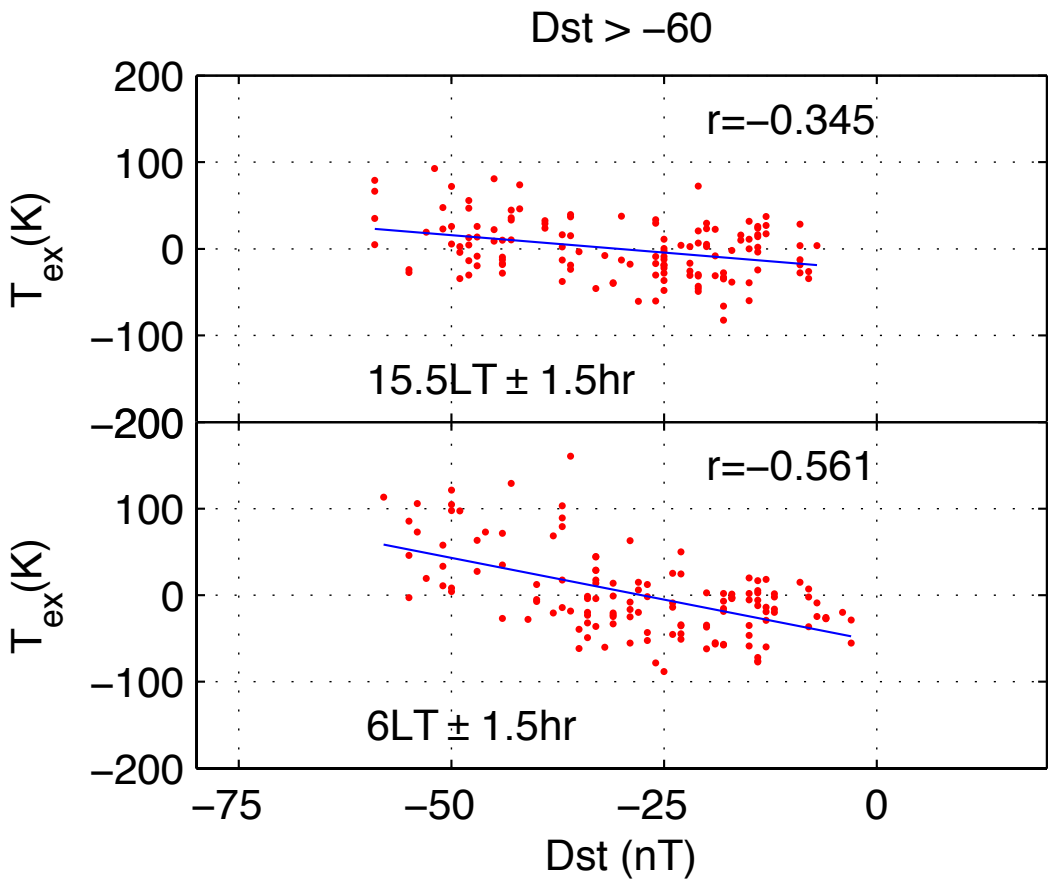

Figure 6. Correlation between T_{ex} and Dst at 1530 LT and 0600 LT, where T_{ex} is computed as the residual T_{ex} after removing EUV effects. The residual is defined as $T - b - d \times D - c_1 \times F - c_2 \times F^2$, where T is original exospheric temperature data, D day number, F the solar EUV at 27–34 nm band, and b, c_1, c_2 are obtained from a least squared fit. Blue lines are linear fitting to the red data points

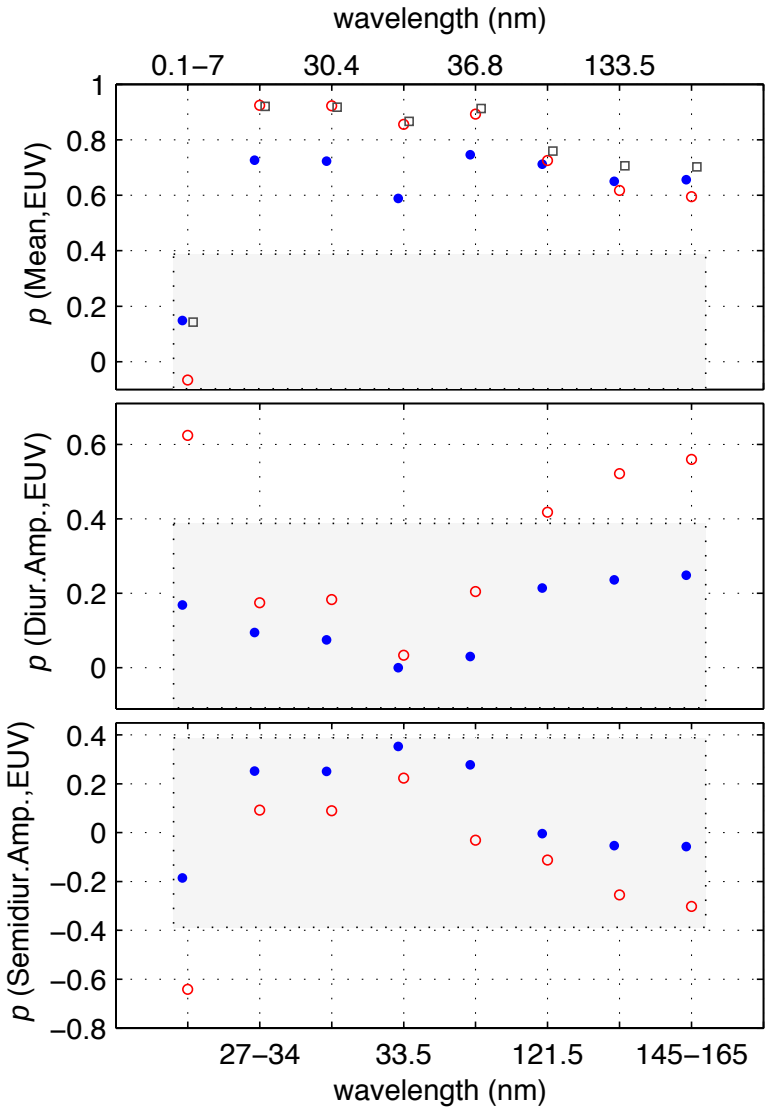

Figure 7. T_{ex} tidal component dependence on solar EUV flux. TIMED/SEE daily average flux at 8 bands is used to evaluate correlations between specific tidal components (mean, top panel; diurnal amplitude, middle panel; semidiurnal amplitude, bottom panel) and EUV flux. Results with a two day time delay (circles) without the delay (dots) are given. Correlation between a composite solar flux proxy E_w at various wavelengths and daily mean T_{ex} is also shown (squares), where E_w contains weighted contributions not only from the current day but also from prior days (see text and Table 1). Shaded areas represent weak correlation, with p-values >0.05 for failure to reject the null hypothesis of no correlation with a sample size of ~ 20.

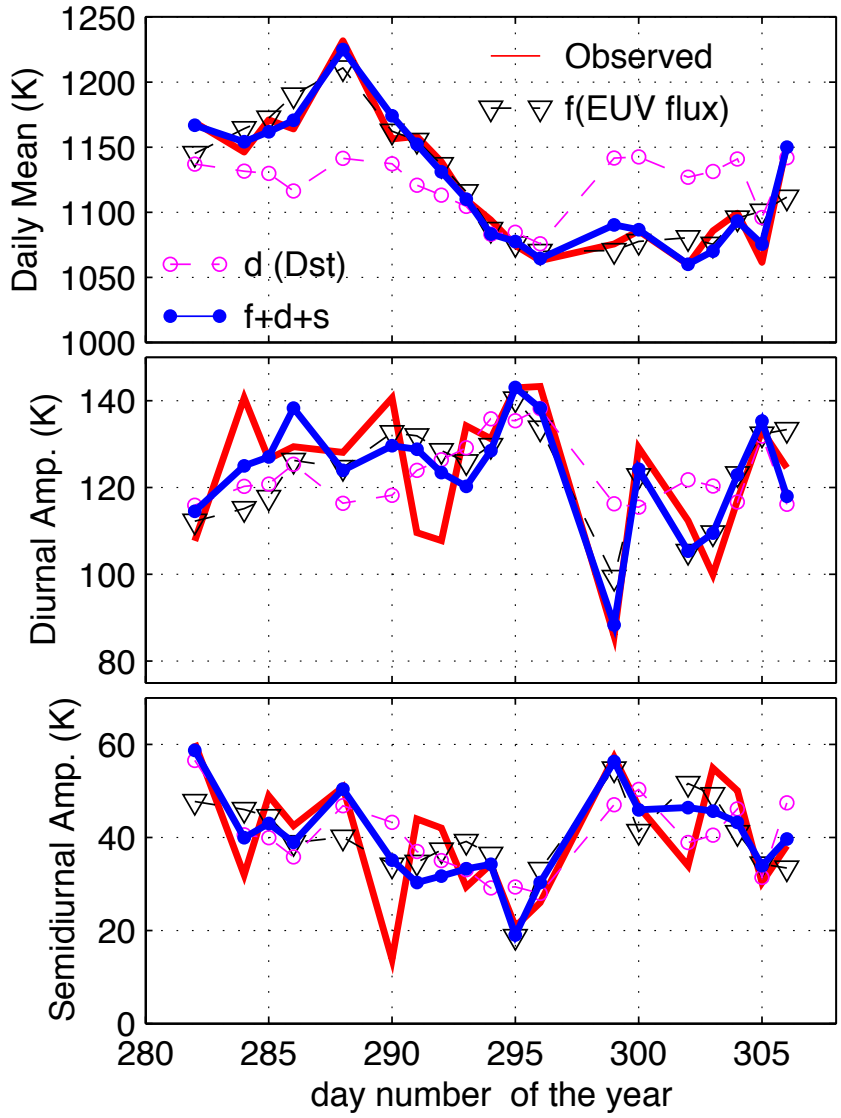

Figure 8. Solar flux, magnetic activity and seasonal effects on T_{ex} daily mean (upper panel), diurnal (middle panel) and semidiurnal (bottom panel) amplitudes. Model functions for the tidal components shown are: **f**: EUV terms; $f_0 + f_1 \times F + f_2 \times F^2$ where F is EUV flux from 2-days in advance at 27–34 nm for T_{ex} daily mean modeling, at 0.1–7 nm band for T_{ex} diurnal and semidiurnal amplitude modeling; **d**: Dst terms, $d_0 + d_1 \times Dst + d_2 \times Dst^2$; **s**: seasonal variation terms, $\sin[2\pi(D + D_0)/365] + \sin[\pi(D + D_{00})/365]$ where D is day number of the year. In these terms, coefficients $f_0, f_1, f_2, d_0, d_1, d_2, D_0, D_{00}$ are determined through least-squares fitting.

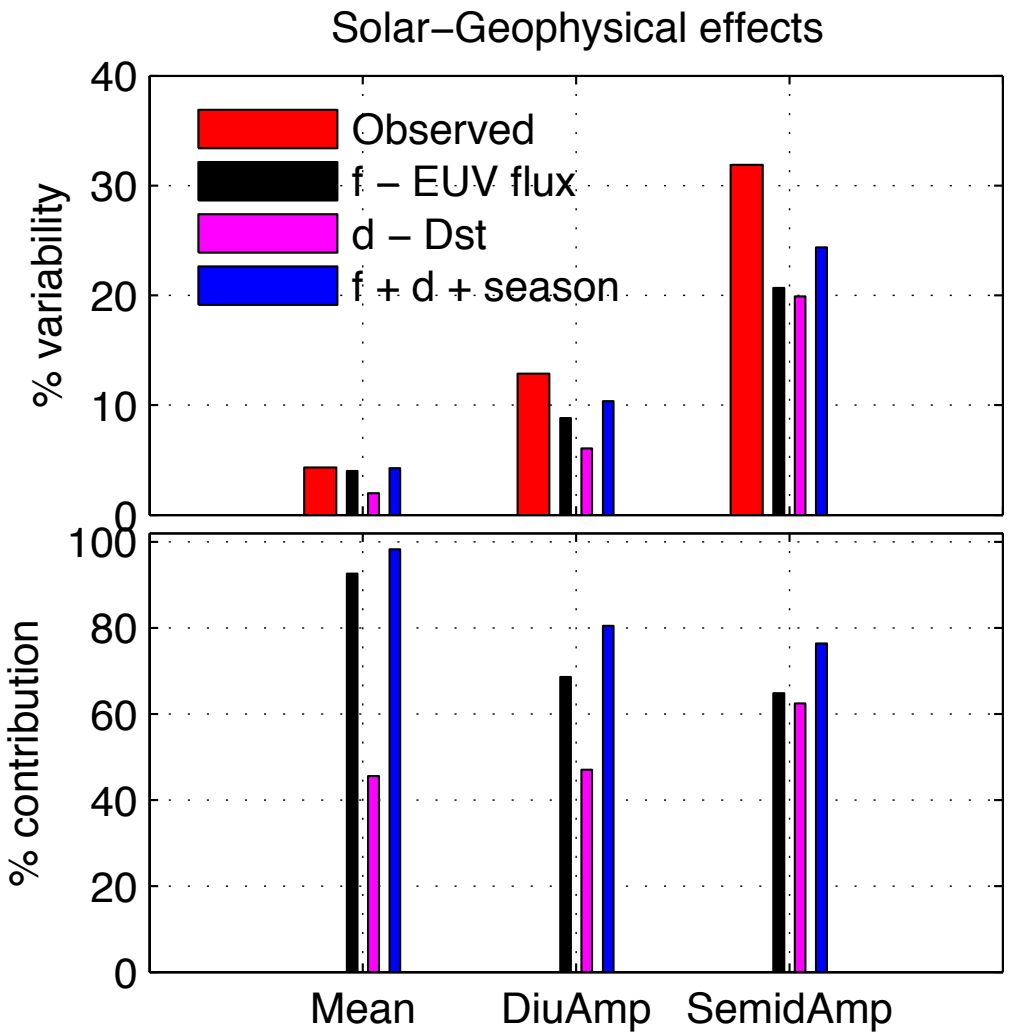

Figure 9. Relative contributions of various factors to day-to-day variability in T_{ex} daily mean, diurnal and semidiurnal amplitudes. Model functions are: f, EUV flux; d, Dst index, and s, season. In the upper panel, a percentage variability of T_{ex} is defined as the standard deviation from the average over the average value. In the bottom panel, the percentage contribution is defined as the standard deviation from the average of empirical model data over the standard deviation from the average of the observational data. The solid line is for observation, and other curves are for results of the modeled variability. The model functions used are the same terms as in Figure 8 (see text).

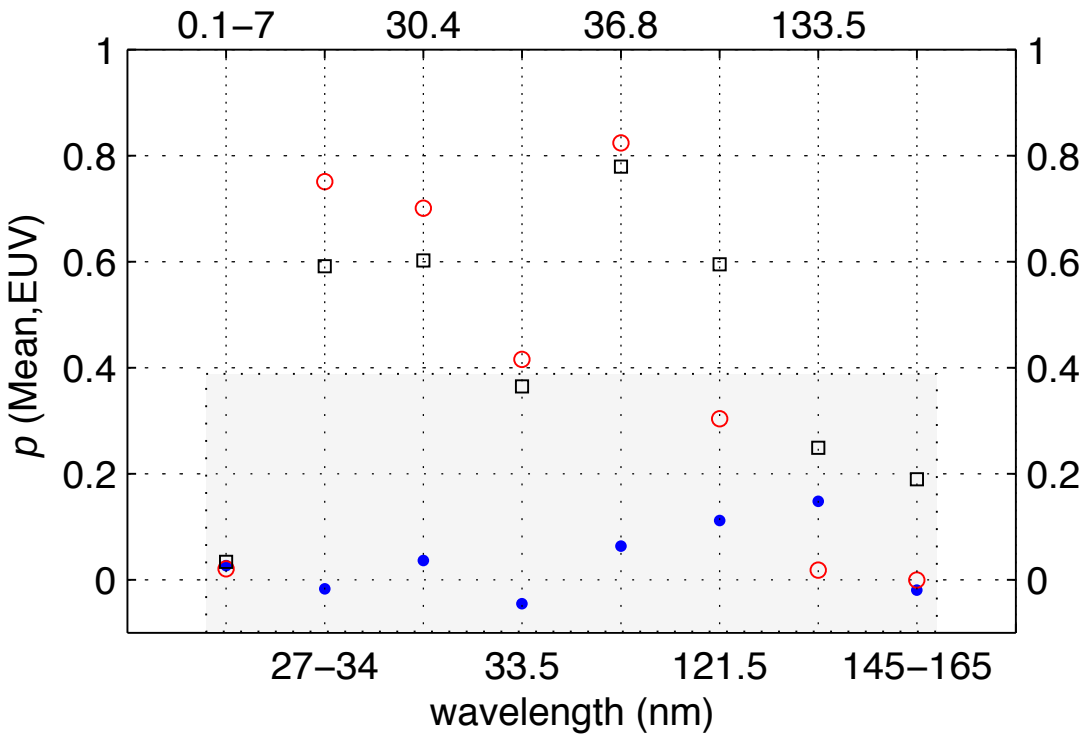

Figure 10. Correlation coefficients between fluctuations in the daily mean T_{ex} and in the solar flux at various wavelengths. Fluctuations are residuals of daily means from the 3-day running means. The solar flux fluctuations are calculated for the same day (dots) as, one day prior (circles) to, and two days prior to (squares) the day of the calculated T_{ex} fluctuation.